

# Are local-field and local-energy approximations appropriate for modeling nanosecond discharges?

Tiago C Dias<sup>1</sup>  and Vasco Guerra\* 

Instituto de Plasmas e Fusão Nuclear, Instituto Superior Técnico, Universidade de Lisboa, Lisboa, Portugal

E-mail: [vguerra@tecnico.ulisboa.pt](mailto:vguerra@tecnico.ulisboa.pt)

Received 25 January 2025, revised 11 March 2025

Accepted for publication 19 March 2025

Published 1 April 2025



CrossMark

## Abstract

A comprehensive solution of the electron kinetics in gas discharges, accounting for dependencies in space, velocity and time, is often unfeasible. Therefore, the electron behavior is frequently coupled to fluid models under one of two assumptions: the local-field approximation (LFA), which equates the electron kinetics to the steady-state calculation with the local and instantaneous value of the reduced electric field; or the local-energy approximation (LEA), in which the rate coefficients and the electron power distribution among different collisional channels depend on the local value of the mean electron energy. In this work, we focus on time-locality to assess the impact of the LFA and LEA assumptions on the calculation of the temporal evolution of the electron kinetics in nanosecond discharges. To do so, we consider an accurate Monte Carlo time-dependent formulation as golden standard. We study electron relaxation in different background gases (air, argon, and mixtures of both) at two pressures (10 and 100 Torr). The LEA generally provides more accurate results than the LFA, with increasing differences at lower pressures, where energy relaxation is slower. The greater accuracy of the LEA comes from the temporal effects introduced by the equation for the mean electron energy, which is absent in the LFA. Opting by the LFA in conditions of slow relaxation can lead to serious degradation of the model results, with errors on the production of excited species up to several tens of percent. Hence, in those scenarios, and when a kinetic approach is not possible, the LEA should be adopted instead of the LFA. The comparison is extended to a two-term time-dependent solver based on a quasi-stationary assumption for the first anisotropy. This method provides a good description of the electron kinetics, except at early times ( $\lesssim 0.2$  ns) at 10 Torr, where the quasi-stationary assumption becomes inaccurate.

Keywords: local-field, local-energy, nanosecond discharges, fluid models, Monte Carlo

<sup>1</sup> Present address: Department of Electrical Engineering, University of Michigan, Ann Arbor, MI, United States of America.

\* Author to whom any correspondence should be addressed.



Original Content from this work may be used under the terms of the [Creative Commons Attribution 4.0 licence](https://creativecommons.org/licenses/by/4.0/). Any further distribution of this work must maintain attribution to the author(s) and the title of the work, journal citation and DOI.

## 1. Introduction

Interest in nanosecond-pulsed discharges (NPDs) is rapidly growing due to their remarkable non-equilibrium properties [1–5]. However, their potential comes with considerable complexity, and a detailed study of the fundamental processes in the discharge is necessary to determine the most efficient configuration for a specific application. NPDs are characterized by very high reduced electric fields,  $E/N$ , that can be as high as  $\sim 1000$  Td, with rising times on the nanosecond timescale. These characteristics pose significant modeling challenges, particularly concerning electron kinetics and their coupling with heavy species.

The electron kinetics in gas discharges can be described by the electron Boltzmann equation (EBE) or by Monte Carlo (MC) simulations. However, in either approach, obtaining a complete solution that accounts for dependencies in space, velocity and time is usually impractical. As a result, the electron behavior is often coupled with fluid models under one of two assumptions [6–11]. The first assumption, the local-field approximation (LFA) or the quasi-stationary approximation, equates the solution of the electron kinetics to the steady-state calculation using the local and instantaneous value of  $E/N$ . This approximation holds when the electron energy relaxation/thermalization is sufficiently fast. The second assumption is the local-energy approximation (LEA), in which the rate coefficients and the electron power distribution along different collisional channels depend on the local value of the mean electron energy. In this case, the EBE is typically solved for a wide range of  $E/N$  under steady-state conditions, and the results are then converted into a lookup table as a function of the mean electron energy. Moreover, an additional equation for the mean electron energy is included, using the input power from the electric field and the power losses obtained from the lookup table.

The focus of this work is on time locality, assessing the impact of the LFA and LEA assumptions on the temporal evolution of electron kinetics in NPDs, where the timescales of energy relaxation can be comparable or even longer than the pulse timescales. The present work is also relevant for the study of streamer discharges at atmospheric pressure, as the electric field at the streamer heads typically involve very rapid changes in  $E/N$ , where locality approximations might not be valid [6, 12, 13]. We consider the formulation within the LisbOn KInetics MC (LoKI-MC) solver [14, 15] as the golden standard for the homogeneous electron kinetics, since it provides the exact solution apart from statistical fluctuations. We then compare this accurate solution against the LFA, LEA and two-term time-dependent approaches in nanosecond pulses, varying the gas pressure (10 and 100 Torr) and considering both molecular ( $N_2$ – $O_2$ ) and atomic (Ar) gases.

The low-temperature plasma community has dedicated significant efforts to the study of the temporal relaxation of the electron kinetics following the instantaneous application of an electric field with fixed amplitude, as thoroughly reviewed by [16]. For instance, investigations have been reported in

He [17, 18], Xe [16, 19], Ne [20], Ar [18, 21],  $N_2$  [17, 20, 22–24],  $N_2$ – $O_2$  (air) [23, 25], and He– $O_2$  [26]. While most investigations focus on selected  $E/N$  values, the comprehensive study conducted by [16] covers a broad range of  $E/N$  fields for Xe, revealing a pronounced dependence of thermalization time on  $E/N$ . Regarding time-dependent  $E/N$  pulses, rather than step-like variations, studies of electron relaxation have been conducted in  $N_2$  and  $N_2$ – $O_2$  by [23], where a time-dependent solution is compared with the LFA, and in He– $O_2$  by [26], where a time-dependent solution is compared with the LEA. However, these studies rely on solving the two-term Boltzmann equation along with a quasi-static approximation for the first anisotropy  $f_1$ . Besides the well-known limitations of the former [14, 27], the latter may not accurately capture the non-equilibrium behavior inherent in steep variations of  $E/N$  [17]. For this reason, the present study extends the analysis to evaluate the accuracy of the two-term time-dependent solution in nanosecond pulses.

The manuscript is structured as follows. Section 2 presents the theoretical background, where section 2.1 outlines the problem at the core of this study and the next three subsections elaborate on the different methods being compared in this research: section 2.2 introduces the time-dependent MC solver, LoKI-MC; section 2.3 discusses the LFA and LEA assumptions; section 2.4 provides a concise overview of the two-term time-dependent solver, LoKI-B. Section 3 presents and discusses the results obtained using the different methods. Section 4 closes the manuscript with final remarks.

## 2. Theoretical background

### 2.1. Problem statement

In this work, we study the temporal evolution of the electron kinetics in nanosecond  $E/N$  pulses under homogeneous conditions. We pay particular attention to selecting configurations that closely resemble those observed in experiments. We use the following analytical expression for  $\frac{E}{N}(t)$  from [23]:

$$\frac{E}{N}(t) = \frac{E_0}{N} \sqrt{\frac{t}{t_{\text{pulse}}}} \exp\left(-\frac{t}{t_{\text{pulse}}}\right), \quad (1)$$

where  $E_0/N = 700$  Td and  $t_{\text{pulse}} = 5$  ns. The corresponding temporal profile of  $E/N$  is illustrated in figure 1. It reaches a maximum value of approximately 300 Td after  $t = 2.5$  ns and decays to a value approximately 100 times lower after 32 ns. This expression mimics well typical profiles of nanosecond discharges; see, for instance, figure 6 in [28] and figure 2 in [29].

It should be noted that this work does not aim at providing an accurate description of the spatiotemporal evolution of nanosecond discharges. For example, high-speed ionization waves are formed in nanosecond discharges, and the pulse of the electric potential moves along the discharge length at a high speed [30–32]. Moreover, the breakdown in nanosecond discharges is often caused by the early development

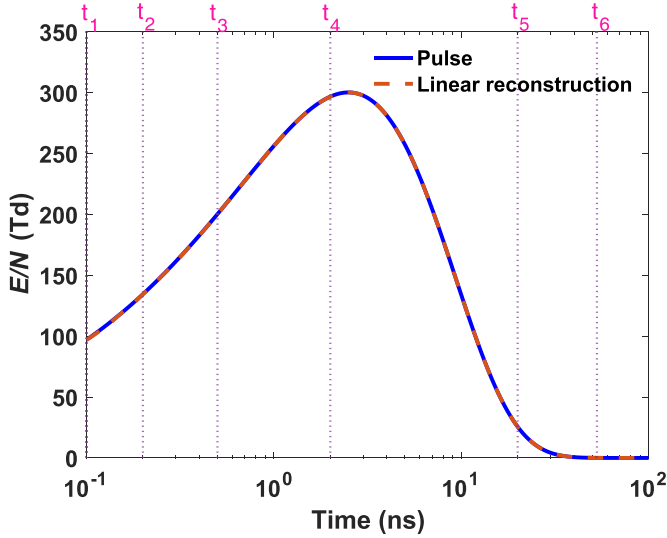


**Figure 1.** Reduced electric field pulse analyzed in this study, as defined by expression (1), with  $E_0/N = 700$  Td and  $t_{\text{pulse}} = 5$  ns. In addition, the figure presents a linear reconstruction of the  $E/N$  pulse, achieved by considering intervals between different slopes of 0.05 ns.

of electron avalanches, which cannot be properly described with a zero-dimensional formulation. Additionally, the electron relaxation at later stages of the electric field pulse can be strongly influenced by electron escape to the surrounding walls. Here, we avoid the intricacies of a simultaneous spatial variation, which is highly system-dependent, and systematically evaluate the impact of different approximations on the fast temporal evolution of electron kinetics using a homogeneous formulation.

To assess the importance of collisionality in electron relaxation, we consider two gas pressure values: 10 and 100 Torr, which are commonly encountered in real discharges [3, 28, 29]. Moreover, we investigate two distinct background gas mixtures, 80%N<sub>2</sub>–20%O<sub>2</sub> (air) and 100%Ar, in order to evaluate the electron kinetics across a wide range of conditions. In air, electron energy relaxation at low-to-medium energies is efficient and controlled by rotational and vibrational collisions, while in argon, it is less efficient and mainly controlled by elastic collisions. Consequently, the effectiveness of time-locality approximations may differ for these two background gas mixtures. In section 3.4, we also address mixtures containing both air and argon. The input cross-section data for the various gases are consistent across the different methods and are taken from the IST-Lisbon database on LXCat [33–36]. As the influence of Coulomb collisions is neglected, the results of the electron kinetics do not depend on the electron density, and the initial value for the electron density is only relevant for the impact on the chemical kinetics, which is addressed in section 3.4. In all cases, the electron density is initialized to  $2.58 \times 10^{18} \text{ m}^{-3}$ , which corresponds to initial ionization degrees of  $8 \times 10^{-6}$  and  $8 \times 10^{-7}$  at 10 and 100 Torr, respectively.

## 2.2. MC time-dependent solver

LoKI-MC simulates the electron kinetics in a background gas under the influence of electric and magnetic fields. The techniques employed in LoKI-MC are detailed in [14, 15, 37]. Therefore, only a brief overview is given here. LoKI-MC tracks the stochastic motion of multiple electrons over time, characterized by free flights punctuated with electron-neutral collisions. The time intervals between collisions are calculated according to the null-collision method, using a trial collision frequency denoted as  $\nu'$ . This frequency must be chosen sufficiently high to overestimate the total collision frequency. The overestimation of the collision frequency is then compensated by introducing null collisions, where no actual interaction takes place. The electron ensemble is synchronized at intervals of  $\nu'^{-1}$  in order to perform the sampling of swarm coefficients.

To ensure a constant number of electrons throughout the simulation, we employ a renormalization technique that adjusts particle counts to balance attachments and ionizations. However, as our goal is to study the temporal evolution across various timescales, we have incorporated the flexibility to track different numbers of electrons over different time intervals. This approach allows us to follow a large number of electrons ( $10^6 - 10^7$ ) during the rise and early decay of the pulse, a moderate number ( $10^5 - 10^6$ ) during the midterm decay, and a smaller number ( $10^4 - 10^5$ ) during the late decay phase. In this way, we can keep the computation time relatively low, around tens of minutes, while ensuring good statistics for each time decade of interest.

When incorporating time-dependent electric fields, the free-flight integration needs to be modified compared to the DC case. We divide the electron motion into smaller intervals, during which the electric field  $E$  varies linearly as  $\mathbf{E}(t_0 + \delta t) = -(E_0 + A\delta t)\mathbf{e}_z$ . The analytical solution for the electron position and velocity between time instants  $t_0$  and  $t_0 + \delta t$  is straightforward. Under the conditions of this study, assuming a single linear variation of the electric field along the free flight is accurate. The quality of this approximation is evident in figure 1, where the linear reconstruction is compared against the original  $E/N$  profile. It is important to note that the time interval used for the linear electric field variation is always equal to or smaller than the synchronization time. In the worst-case scenario under study, involving argon at 10 Torr, the synchronization time is approximately 0.01 ns. In the linear reconstruction example, we use a time interval five times larger than the maximum synchronization time, specifically 0.05 ns, and the reconstruction still matches the original pulse very well. To further confirm the accuracy of this approach, we have divided the motion into 100 smaller parts and found no visible deviation of the results from the single-linear case.

## 2.3. The local-field and LEAs

For a rigorous discussion on how the local-field and LEAs appear in the context of fluid modeling, starting from the

general EBE, the reader is referred to the works by [6] and [8]. Investigations performed under the LFA can be found, e.g. in [28, 38–40], and under the LEA in [9, 41–46].

The LFA involves calculating the steady-state electron kinetics while assuming locality in both space and time. In this case, the electron energy distribution function (EEDF), rate coefficients and transport parameters explicitly depend on the local and instantaneous value of  $E/N$ . For a homogeneous system, this approximation remains valid as long as the electron energy relaxation frequency ( $\nu_\epsilon$ ) is much larger than the characteristic frequency of  $E/N$  variation ( $\nu_{E/N}$ ):

$$\frac{\nu_\epsilon}{\nu_{E/N}} \gg 1, \quad \nu_{E/N} \equiv \left| \frac{d(E/N)}{dt} \right| / (E/N). \quad (2)$$

Note that the calculation of  $\nu_{E/N}$  involves the relative variation of the reduced electric field with time. In principle, if the numerical precision is sufficient to prevent artificially high values of  $\nu_{E/N}$  at low reduced electric fields, the comparison between  $\nu_\epsilon$  and  $\nu_{E/N}$  in equation (2) remains useful. When spatial variations are relevant, in addition to the previous condition, the mean free path for energy relaxation ( $\lambda_\epsilon$ ) must be much smaller than the minimum characteristic length for the variations of both  $E/N$  and the background gas mixture ( $\lambda_{\text{spatial}}$ ). Although the same conditions must also be verified for momentum relaxation, verifying the energy relaxation condition is sufficient, as the momentum relaxation frequency ( $\nu_m$ ) is much larger than  $\nu_\epsilon$  under virtually all conditions.

In the LEA, an equation for the mean electron energy  $\langle \epsilon \rangle$  is introduced, which can be expressed as follows [6, 8]:

$$\frac{\partial (n_e \langle \epsilon \rangle)}{\partial t} = en_e \mu_e E^2 + n_e P_{\text{coll}} + \Theta_{\text{transp}}. \quad (3)$$

Here,  $n_e$  is the electron density,  $\mu_e$  is the electron mobility and  $P_{\text{coll}}$  is the net power transferred by collisions per electron. The term  $\Theta_{\text{transp}}$  represents a transport contribution that we omit since our focus is on temporal effects. Therefore, in homogeneous conditions, the equation for mean energy becomes:

$$\frac{d\langle \epsilon \rangle}{dt} = e \mu_e E^2 + P_{\text{coll}} - \langle \nu_{\text{eff}} \rangle \langle \epsilon \rangle, \quad (4)$$

where  $\langle \nu_{\text{eff}} \rangle \equiv dn_e/dt$  denotes the average effective ionization frequency and  $-\langle \nu_{\text{eff}} \rangle \langle \epsilon \rangle$  represents the contribution of the electron density growth. In the context of the LEA,  $\mu_e$ ,  $P_{\text{coll}}$  and  $\nu_{\text{eff}}$  are considered functions of the mean electron energy  $\langle \epsilon \rangle$ . The approximated dependencies for these quantities are derived by solving steady-state electron kinetics across a wide range of  $E/N$  and then parameterizing the results as functions of  $\langle \epsilon \rangle$  [7, 42]. The validity domain of the LEA is less well-defined than in the LFA, but due to the use of parameterized steady-state mobilities in the Joule heating term, at least the momentum transfer must be much faster than the rate of change of the electric field:

$$\frac{\nu_m}{\nu_{E/N}} \gg 1. \quad (5)$$

Similarly, in the case of spatial variations, the mean free path for momentum-transfer ( $\lambda_m$ ) should be much smaller than  $\lambda_{\text{spatial}}$ .

Lastly, in this work, we employ LoKI-MC for the accurate solution of steady-state electron kinetics, required for both the LFA and LEA, ensuring that any deviations from the exact time-dependent solutions arise due to the time-locality approximations.

#### 2.4. Two-term time-dependent solver

In addition to the calculations described in the previous sections, we employ the electron kinetics solver LoKI-B to solve the time-dependent EBE under the two-term approximation, as detailed by Tejero-del-Caz *et al* [23, 47], aiming to evaluate the quality of the approach. For completeness, we provide an overview of the primary approximations involved in LoKI-B, while avoiding intricate mathematical details.

As a starting point, we assume that the *homogeneous* electron velocity distribution function, denoted as  $f_e(\mathbf{v}, t)$ , can be expanded in Legendre polynomials with respect to the velocity vector  $\mathbf{v}$ :

$$f_e(\mathbf{v}, t) = \sum_l f_l(v, t) P_l(\cos \theta) \simeq f_0(v, t) + f_1(v, t) \cos \theta. \quad (6)$$

Here,  $P_l(\cos \theta)$  is the Legendre polynomial of order  $l$ ;  $\theta$  is the polar angle of  $\mathbf{v}$  relative to the anisotropy direction (defined by the electric field);  $f_0$  and  $f_1$  correspond to the isotropic and first anisotropic components of the electron velocity distribution function, respectively. When written in terms of energy  $u$ , the isotropic part  $f_0(u, t)$  corresponds to the EEDF, normalized such that  $\int_0^\infty f_0(u, t) \sqrt{u} du = 1$ . Let us note that neglecting higher order terms in the Legendre expansion is only accurate if anisotropies are sufficiently low.

Upon inserting this expansion into the homogeneous EBE, we derive two equations: one for  $\frac{\partial f_0}{\partial t}$ , which depends on  $f_0$  and  $f_1$ , and another for  $\frac{\partial f_1}{\partial t}$ , which also depends on  $f_0$  and  $f_1$ . For higher order Legendre expansions, the second equation would involve  $f_2$  as well. Additionally, we assume that the term  $\frac{\partial f_1}{\partial t}$  can be neglected and is set to zero. This approximation assumes that the relaxation of  $f_1$  occurs significantly faster than that of  $f_0$  and the electric field  $E$ , and holds when  $\nu_m/\nu_\epsilon \gg 1$  (typically the case), together with condition (5). Under this assumption,  $f_1$  can be expressed as a function of  $f_0$ , and  $\frac{\partial f_0}{\partial t}$  can be simplified to depend solely on  $f_0$ . Then, the equation for  $f_0$  can be solved over time. It is worth noting that the quasi-static assumption for  $f_1$  serves only to simplify the complexity of the system and is independent of the two-term approximation. However, in regions where the electric field variation is steep and condition (5) does not hold, this assumption may impact the accuracy of the solution, as demonstrated in the next section.

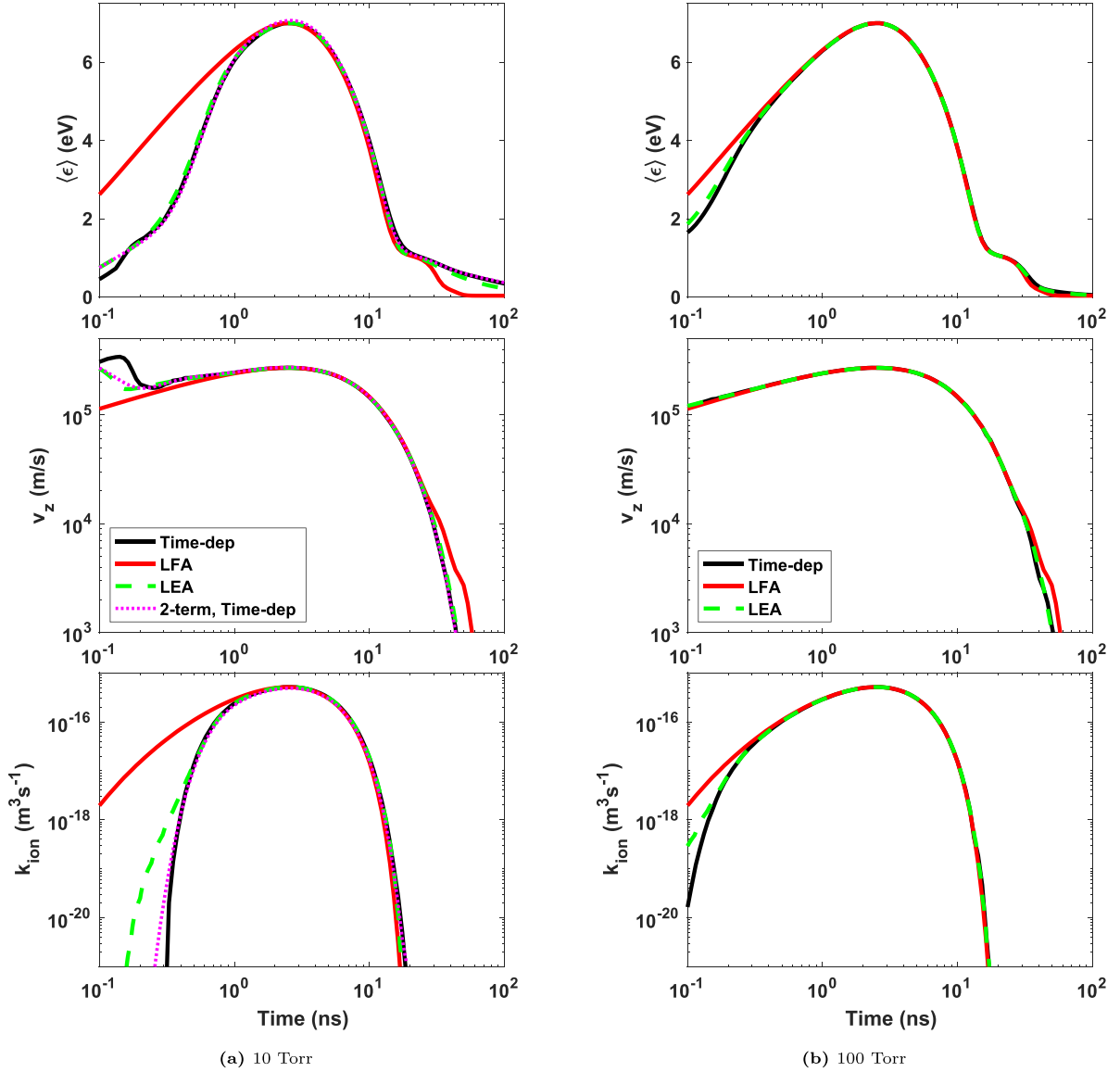


**Figure 2.** Temporal evolution of the mean electron energy ( $\langle \epsilon \rangle$ ), drift velocity ( $v_d$ ) and ionization coefficient ( $k_{ion}$ ), in air, at (a) 10 Torr and (b) 100 Torr conditions.

### 3. Results

This section presents the results of the electron kinetics under the conditions outlined in section 2.1, comparing the rigorous MC time-dependent approach with the other approximate methods described in sections 2.2–2.4. We begin by analyzing the temporal evolution of the electron swarm coefficients. Next, we discuss the importance of quantifying the characteristic relaxation frequencies, and examine the EEDFs at various time instants. Finally, in section 3.4, we showcase the impact of these assumptions when coupling the electron kinetics with the chemical kinetics, focusing on the production of reactive oxygen and nitrogen species (RONS).

#### 3.1. Electron swarm coefficients

We start by detailing the temporal evolution of the electron swarm coefficients in air, under the application of the  $E/N$  pulse depicted in figure 1. Figure 2 illustrates the evolution of the mean electron energy ( $\langle \epsilon \rangle$ ), drift velocity ( $v_d$ ) and ionization coefficient ( $k_{ion}$ ), up to 100 ns, for conditions at (a) 10 Torr and (b) 100 Torr.

At 10 Torr (see figure 2(a)), the evolution of  $\langle \epsilon \rangle$  calculated by the LFA differs significantly from the rigorous time-dependent MC approach. This discrepancy arises because at lower pressures electrons do not collide rapidly enough to adapt to fast  $E/N$  variations, and condition (2) is not verified. After approximately 2 ns, the LFA and time-dependent

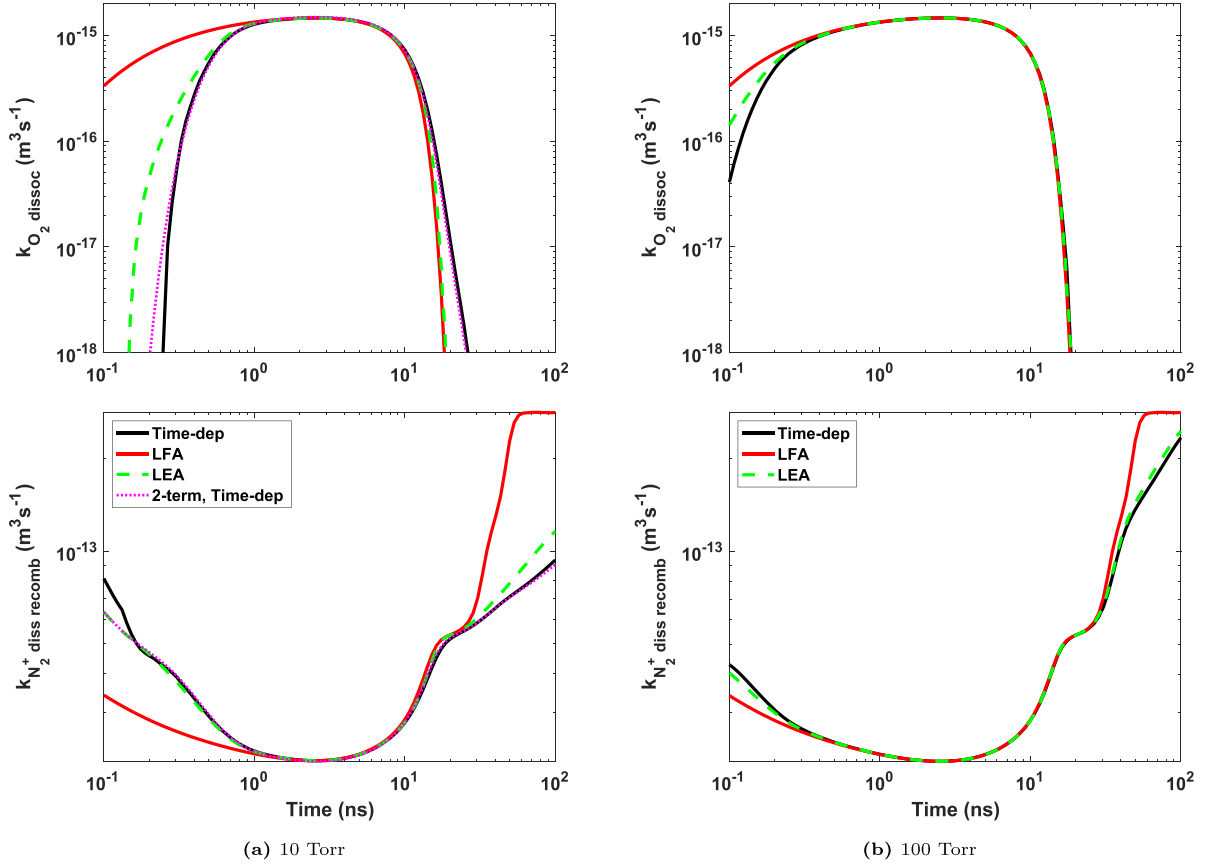


**Figure 3.** Temporal evolution of electron-impact  $\text{O}_2$  dissociation (top),  $e + \text{O}_2(\text{X}) \rightarrow e + 2\text{O}({}^3\text{P})$ , and  $\text{N}_2^+$  dissociative recombination (bottom),  $e + \text{N}_2^+ \rightarrow 2\text{N}$ , in air, at (a) 10 Torr and (b) 100 Torr conditions.

calculations begin to converge. However, around 20 ns, when the  $E/N$  pulse has decayed to 25 Td, the LFA again deviates from the time-dependent solution. A similar trend is found for  $v_d$ . Notably, during the initial 2 ns, the LFA significantly overestimates electron production, quantified by the value of  $k_{\text{ion}}$ .

Both the LEA and two-term time-dependent approaches capture  $\langle \epsilon \rangle$ ,  $v_d$  and  $k_{\text{ion}}$  results closer to the time-dependent MC results than the LFA. Interestingly, the LEA and two-term outcomes of  $\langle \epsilon \rangle$  and  $v_d$  exhibit striking similarity during the first 0.2 ns. This resemblance arises due to shared approximations in the two methods: (i) the two-term time-dependent solution calculates the first anisotropy  $f_1$  using a quasi-static approximation, wherein  $f_1$  depends on the instantaneous  $E/N$  and  $f_0$  values; (ii) in the LEA approach, the electron mobility  $\mu_e$  (linked to  $f_1$ ) is computed using steady-state calculations parameterized as a function of the mean electron energy. These approximations are based on the condition (5), which is not valid during the early pulse rise, and they also influence the  $\langle \epsilon \rangle$  evolution, as the Joule heating power depends on  $f_1$  or  $\mu_e$ . Nevertheless, both the LEA and two-term time-dependent yield satisfactory results after 0.2 ns. In the late pulse-decay phase, the two-term time-dependent solution aligns closely with the rigorous solution, while the LEA slightly deviates, although still closer than the LFA.

At 100 Torr (see figure 2(b)), where electron collisions are significantly more frequent than at 10 Torr, the LFA is valid over a broader time interval, being satisfactory from 0.4 ns to 30 ns. For clarity in the presentation of results, the two-term time-dependent solution is omitted from the figure in this case, although it closely matches the MC time-dependent calculation. Similarly to the 10 Torr case, the LEA offers a better description than the LFA.

To further demonstrate the influence of time-locality approximations on electron-impact rate coefficients with relevance on the plasma chemistry, figure 3 illustrates the temporal evolution of electron-impact  $\text{O}_2$  dissociation (top),  $e + \text{O}_2(\text{X}) \rightarrow e + 2\text{O}({}^3\text{P})$ , and  $\text{N}_2^+$  dissociative recombination (bottom),  $e + \text{N}_2^+ \rightarrow 2\text{N}$ . At 10 Torr, during the initial nanosecond,  $\text{O}_2$  dissociation is strongly overestimated by the LFA and  $\text{N}_2^+$  dissociative recombination is underestimated. After 10–20 ns,  $\text{O}_2$  dissociation is underestimated by the LFA and  $\text{N}_2^+$  dissociative recombination is considerably overestimated. The pronounced overestimation of dissociative recombination must be highlighted, as it is one of the primary processes leading to electron loss. Therefore, the LFA may predict a much faster decay of electrons, which subsequently influences the overall chemistry during the late decay phase, as demonstrated in section 3.4. Once again, the LEA provides a much better result, albeit not perfect. At 100 Torr, the differences

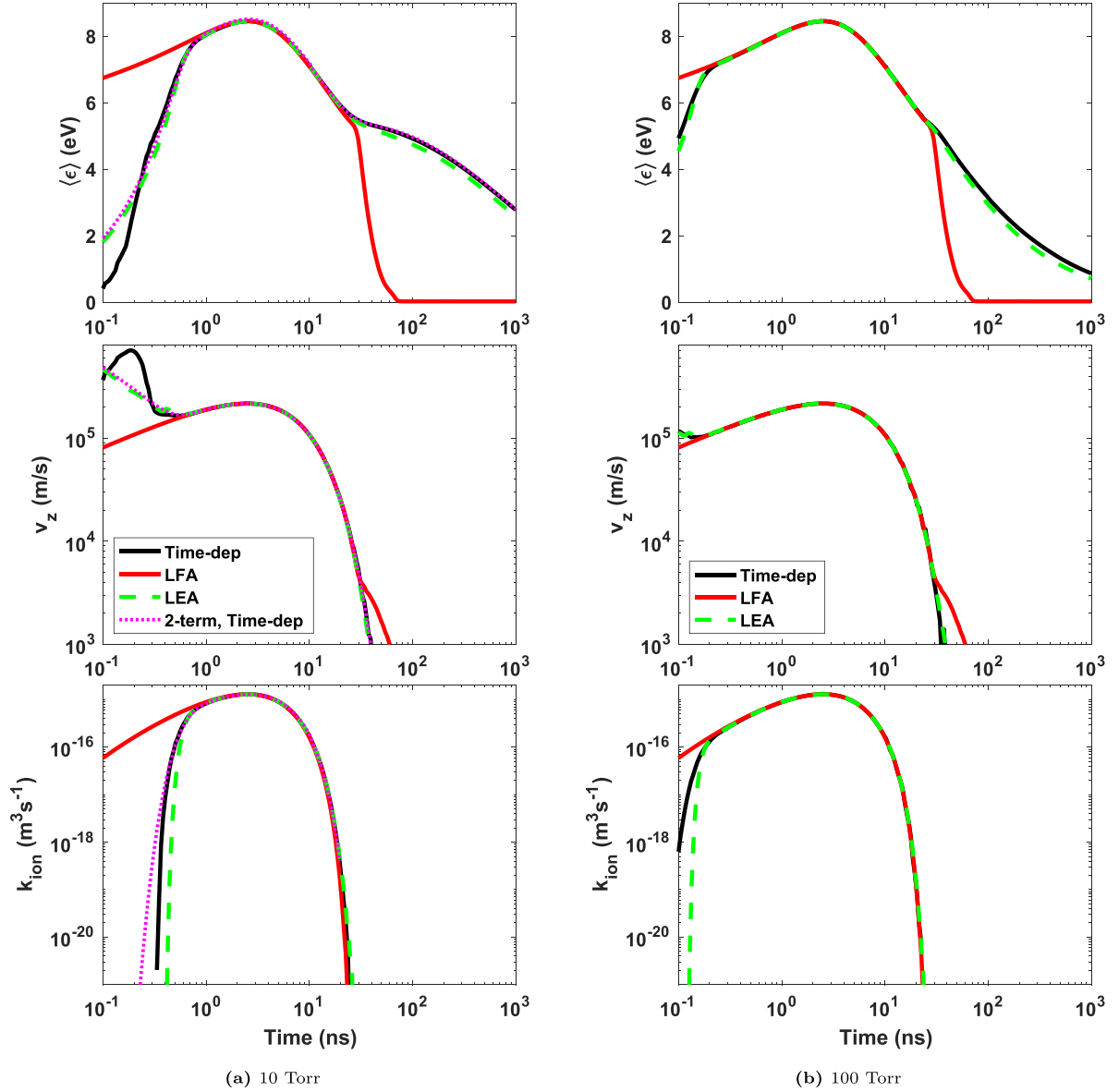


**Figure 4.** Temporal evolution of the mean electron energy ( $\langle \epsilon \rangle$ ), drift velocity ( $v_d$ ) and ionization coefficient ( $k_{ion}$ ), in argon, at (a) 10 Torr and (b) 100 Torr conditions.

between the various approaches are smaller yet still discernible.

Next, we proceed to analyze the behavior in argon, where energy relaxation is generally much weaker. Figure 4 illustrates the temporal evolution of  $\langle \epsilon \rangle$ ,  $v_d$ , and  $k_{ion}$ , up to  $1 \mu s$ , for conditions at (a) 10 and (b) 100 Torr. The disparity between the LFA and rigorous time-dependent methods is even more pronounced in argon compared with air. The strong inaccuracy of the LFA in describing the late decay arises from the low energy relaxation frequency of argon, as detailed in the following section. Both the LEA and two-term time-dependent solutions provide much better descriptions than the LFA. However, similarly to observations in air, neither of these approaches can accurately capture the steep increase of  $v_d$  during the

first 0.2 ns. The two-term time-dependent solution matches the late decay perfectly, while the LEA yields satisfactory results. At 100 Torr, the LFA shows good results during the pulse rise after 0.3 ns but still fails notably for times longer than 30 ns, due to the assumed instantaneous adjustment of the EEDF to the reduced field when the energy relaxation is actually slow.

In general, the results presented in this section show that, despite the highest  $E/N$  derivative occurring during the pulse rise, the use of different locality approximations can have a greater impact during the  $E/N$  decay than during the rise, since the mean electron energy can remain elevated for an extended period of time. These findings are further clarified in the following sections.

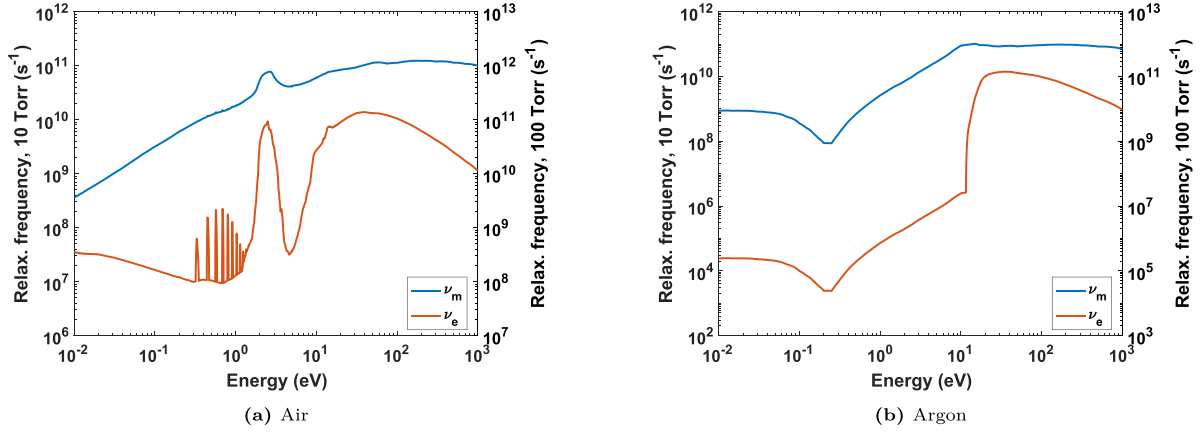


**Figure 5.** Energy-dependent frequencies of momentum transfer ( $\nu_m$ ) and energy relaxation ( $\nu_\epsilon$ ), in (a) air and (b) argon, at gas pressures of 10 and 100 Torr (left and right axis, respectively).

### 3.2. Characteristic relaxation frequencies

The analysis of the characteristic relaxation frequencies provides further insight into the deviations of different time-locality approximations from the accurate time-dependent solution and establishes quantitative criteria to anticipate their domains of validity. The relaxation efficiency is determined by both the frequency of momentum transfer ( $\nu_m$ ) and the frequency of energy relaxation ( $\nu_\epsilon$ ). These frequencies can be estimated in the following way [48, 49]:

$$\nu_m(\epsilon) = \sqrt{\frac{2\epsilon\epsilon}{m}} \sum_i n_i \sigma_{m,i}(\epsilon), \quad (7)$$

$$\nu_\epsilon(\epsilon) = \sqrt{\frac{2\epsilon\epsilon}{m}} \left\{ \sum_{i \in \text{elast}} \frac{2m}{M_i} n_i \sigma_i(\epsilon) + \sum_{i \in \text{rot, vib, elec, ion}} \frac{|\Delta\epsilon_i|}{\epsilon} n_i \sigma_i(\epsilon) + \sum_{i \in \text{att}} n_i \sigma_i(\epsilon) \right\}. \quad (8)$$

Here,  $\epsilon$  is the electron energy in eV;  $n_i$  and  $M_i$  are the density and mass of the heavy target in collision  $i$ ;  $\sigma_{m,i}(\epsilon)$  and  $\sigma_i(\epsilon)$  are the corresponding momentum-transfer and integral cross sections, respectively, and they match under the assumption of isotropic scattering;  $\Delta\epsilon_i$  is the inelastic energy transfer, which is negative for inelastic collisions and positive for superelastic collisions. As expressed in equations (7) and (8), for momentum transfer, the sum is equally performed over all collision types, whereas for energy relaxation, the sum is separated into three parts: (i) elastic collisions; (ii) rotational, vibrational, electronic and ionization collisions; (iii) attachment collisions.

The energy-dependent frequencies  $\nu_m$  and  $\nu_\epsilon$  are depicted in figure 5, considering both pressures of 10 and 100 Torr and for the two background mixtures: (a) air and (b) argon. In both gases,  $\nu_m \gg \nu_\epsilon$ , which is expected. Furthermore,  $\nu_m$  and  $\nu_\epsilon$  show a strong dependence on the electron energy. In the case of air,  $\nu_m$  exhibits a monotonically increasing trend with electron energy, except for a localized structure between 1 and 4 eV, where vibrational excitation of  $\text{N}_2$  dominates. The spikes

in  $\nu_\epsilon$  starting from 0.3 eV are attributed to resonance peaks in vibrational excitation of  $\text{O}_2$ , while the relatively large values of  $\nu_\epsilon$  between 1 and 4 eV are due to vibrational excitation of  $\text{N}_2$ . The dip in  $\nu_\epsilon$  at around 4.5 eV is a consequence of reduced vibrational excitation, and the rapid increase thereafter is associated with the excitation of higher-energy electronic states and ionization. The significant decrease in  $\nu_\epsilon$  after 100 eV is due to diminutions in both the magnitude of cross-sections and the ratios  $\frac{|\Delta\epsilon_i|}{\epsilon}$ . In argon, momentum transfer and energy relaxation are entirely controlled by elastic collisions up to approximately 12 eV. Consequently, in this interval, the trends of  $\nu_m$  and  $\nu_\epsilon$  mirror the shape of the elastic cross section, featuring the well-known Ramsauer minimum around 0.25 eV. Moreover, in the same region,  $\nu_\epsilon/\nu_m = \frac{2m}{M} \approx 2.7 \times 10^{-5}$ , indicating that energy relaxation is much less efficient than momentum transfer. The sharp increase of  $\nu_\epsilon$  after 12 eV is caused by the emergence of strong inelastic processes, including electronic excitations and ionization.

Figure 6 compares the temporal evolutions of the typical  $E/N$  variation frequency, defined as  $\nu_{E/N} = \left| \frac{d(E/N)}{dt} \right| / (E/N)$ , and the energy-averaged frequencies  $\langle \nu_m \rangle$  and  $\langle \nu_\epsilon \rangle$ , for both (a) air and (b) argon, at pressures of 10 and 100 Torr. In both air and argon,  $\langle \nu_m \rangle$  and  $\langle \nu_\epsilon \rangle$  exhibit variations across different orders of magnitude, corresponding to distinct mean electron energies. Starting with the analysis at 10 Torr, in both air and argon, the condition  $\nu_{E/N}/\langle \nu_m \rangle \ll 1$  is not satisfied during the initial 0.2 ns. Therefore, the assumption of instantaneous relaxation of anisotropies is invalid within this interval, and the LEA and two-term time-dependent approaches provide inaccurate results. However, this assumption begins to hold for later times. Concerning energy relaxation during the pulse rise,  $\nu_{E/N}/\langle \nu_\epsilon \rangle \ll 1$  only occurs after 1 ns, which is roughly when the LFA provides reasonable results. During the pulse decay, as electron energy and energy relaxation decrease significantly,  $\nu_{E/N}/\langle \nu_\epsilon \rangle \gtrsim 1$  after 10–20 ns, causing local energy relaxation to break down and the LFA to become inaccurate. However, momentum transfer remains sufficiently fast, with  $\nu_{E/N}/\langle \nu_m \rangle \ll 1$ . At 100 Torr, momentum transfer is efficient throughout the pulse in both gases. The increased collisionality

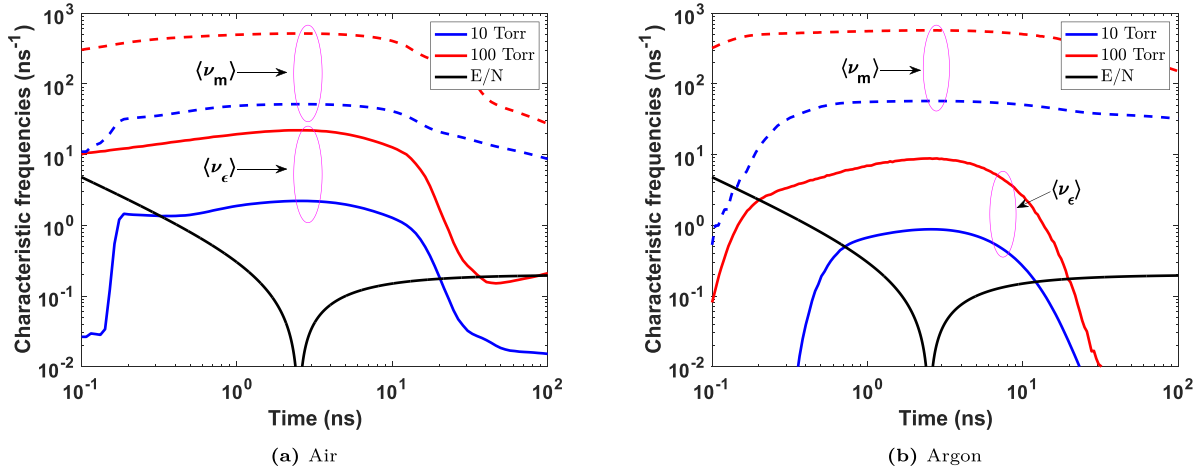


**Figure 6.** Temporal evolution of energy-averaged frequencies of momentum transfer ( $\langle \nu_m \rangle$ , dashed) and energy relaxation ( $\langle \nu_e \rangle$ , full), at 10 and 100 Torr, in (a) air and (b) argon. The characteristic frequency of  $E/N$  variation ( $\nu_{E/N}$ ) is represented with full black lines.

enhances energy relaxation, but it remains insufficient to make the LFA accurate during the pulse rise and, specially, during the pulse decay. This discrepancy is more pronounced in argon, where for times longer than 20 ns,  $\nu_{E/N}/\langle \nu_e \rangle \gg 1$ .

### 3.3. Distribution functions

The strong energy dependence of relaxation frequencies, as demonstrated in figure 5, suggests that the time-dependent EEDFs can exhibit transient shapes significantly divergent from the typical steady-state ones.

Figure 7 showcases the EEDFs in air at six time points  $t_1$ – $t_6$  throughout the pulse (marked in figure 1), considering the lower pressure of 10 Torr. The corresponding instantaneous values of  $E/N$  are indicated in the captions of figure 7. At  $t_1 = 0.1$  ns and  $t_2 = 0.2$  ns, neither the LFA, the LEA nor the two-term time-dependent approaches capture the transient characteristics of the distribution. By  $t_3 = 0.5$  ns, the LEA and two-term time-dependent approaches begin to provide an accurate description, as momentum transfer is fast compared with the field variation. At  $t_4 = 2$  ns, temporal locality induces convergence among all four approaches. The minor deviation of the two-term time-dependent solution stems from a breakdown of the two-term approximation and not from temporal non-locality. By  $t_5 = 20$  ns, when the pulse has decayed to  $E/N \simeq 25$  Td, the various approximate approaches still predict well the values of the distribution up to 3 eV, but the LFA and LEA fail thereafter due to a decrease of energy-relaxation frequency (see figure 5(a)). This pronounced non-equilibrium characteristic can only be captured with kinetic descriptions like MC or two-term time-dependent approaches. Lastly, at  $t_6 = 53$  ns, with  $E/N$  having fallen to 0.05 Td, the LFA severely fails, and the LEA can only crudely replicate the distribution shape. The intriguing features in the EEDF are directly associated with spikes in  $\nu_e$ , as shown in figure 5(a). Evidently, the differences in the EEDFs between the different approximations directly translate into the differences in the rate coefficients for  $O_2$  dissociation and  $N_2^+$  recombination shown in figure 3, which will have an impact in any time-dependent

description of the plasma, as demonstrated in the following section.

Figure 8 depicts the EEDFs in argon at the same time instants  $t_1$ – $t_6$  and 10 Torr. For the initial four time points, conclusions parallel those in air. At  $t_1 = 0.1$  ns and  $t_2 = 0.2$  ns, the non-equilibrium profile cannot be described with the three approximate methods. At  $t_3 = 0.5$  ns, the LEA and two-term time-dependent techniques already give good results. At  $t_4 = 2$  ns, electron kinetics attains quasi-static conditions and all time-locality approximations are valid. By  $t_5 = 20$  ns, the LFA fails in the high-energy tail, while the LEA and two-term time-dependent methods match the rigorous time-dependent solution. Finally, at  $t_6 = 53$  ns, the LFA collapses and the LEA still gives reasonably good results, albeit with an overestimation of the high-energy tail. Again, the breakdown of the LFA may have a significant impact on the chemical description in the after-pulse phase.

### 3.4. Impact on chemical kinetics

The previous section highlights significant differences in the EEDFs based on the assumptions made for the electron kinetics solution. Since the electron-impact rate coefficients used in chemical kinetics are calculated by integrating the cross-section weighted by the EEDF, it is expected that the use of time-locality assumptions may significantly influence chemical kinetics. Here, we aim to quantify the error introduced by the LFA and LEA in chemical kinetics compared to the accurate time-dependent solution, focusing on the RONS. To achieve this error quantification, we use the results of the electron kinetics calculation as input for a system of rate-balance equations that solve the evolution of the chemical kinetics of discharges involving air and air-argon mixtures. For the  $E/N$  pulse, we use the same analytical expression (1), but with slightly different parameters from the previous sections: for 10 Torr,  $E_0/N = 700$  Td and  $t_{\text{pulse}} = 10$  ns, and for 100 Torr,  $E_0/N = 400$  Td and  $t_{\text{pulse}} = 5$  ns, to increase (decrease) the overall electron-impact ionization at lower (higher) pressures. Additionally, to analyze the accumulation of errors over

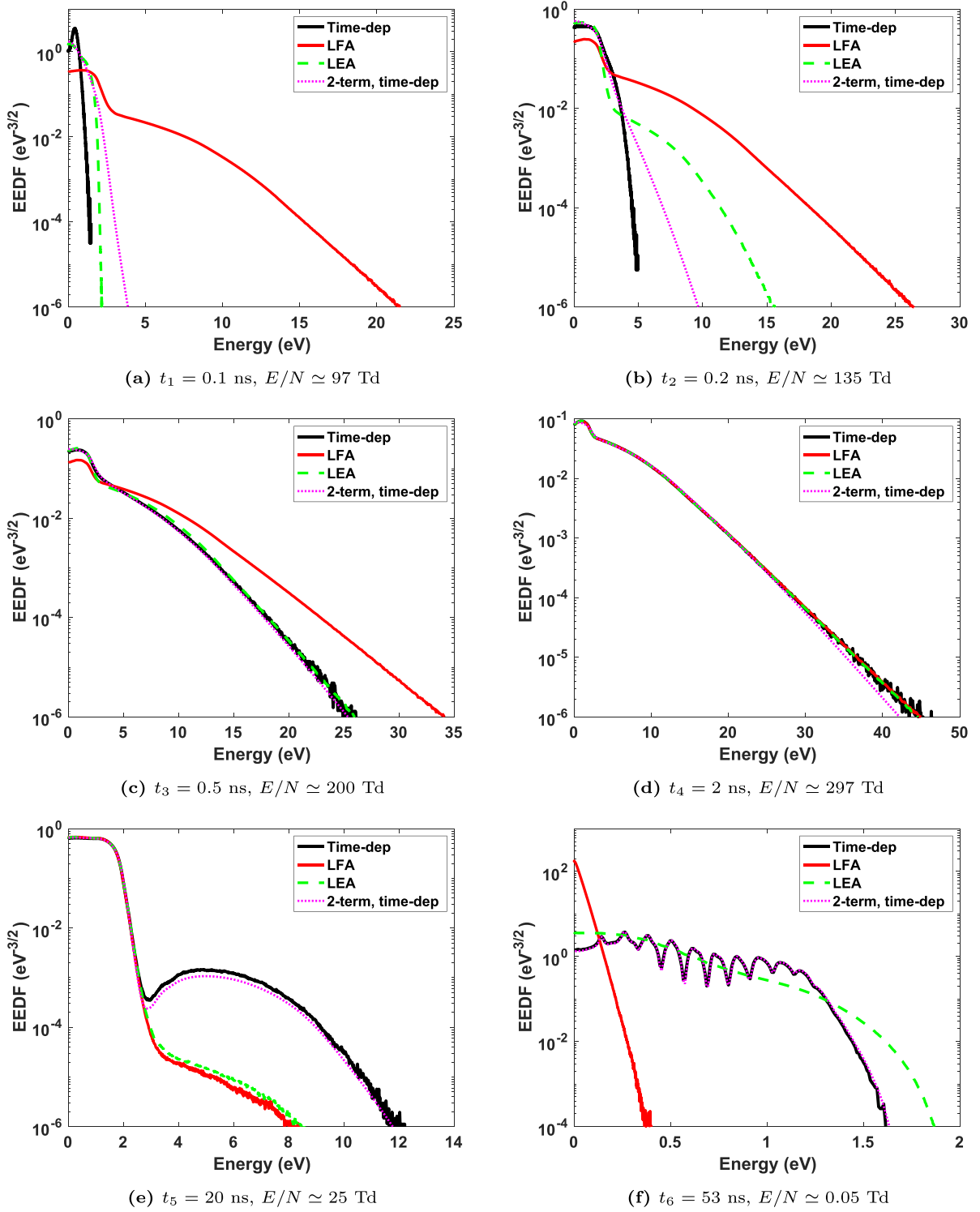
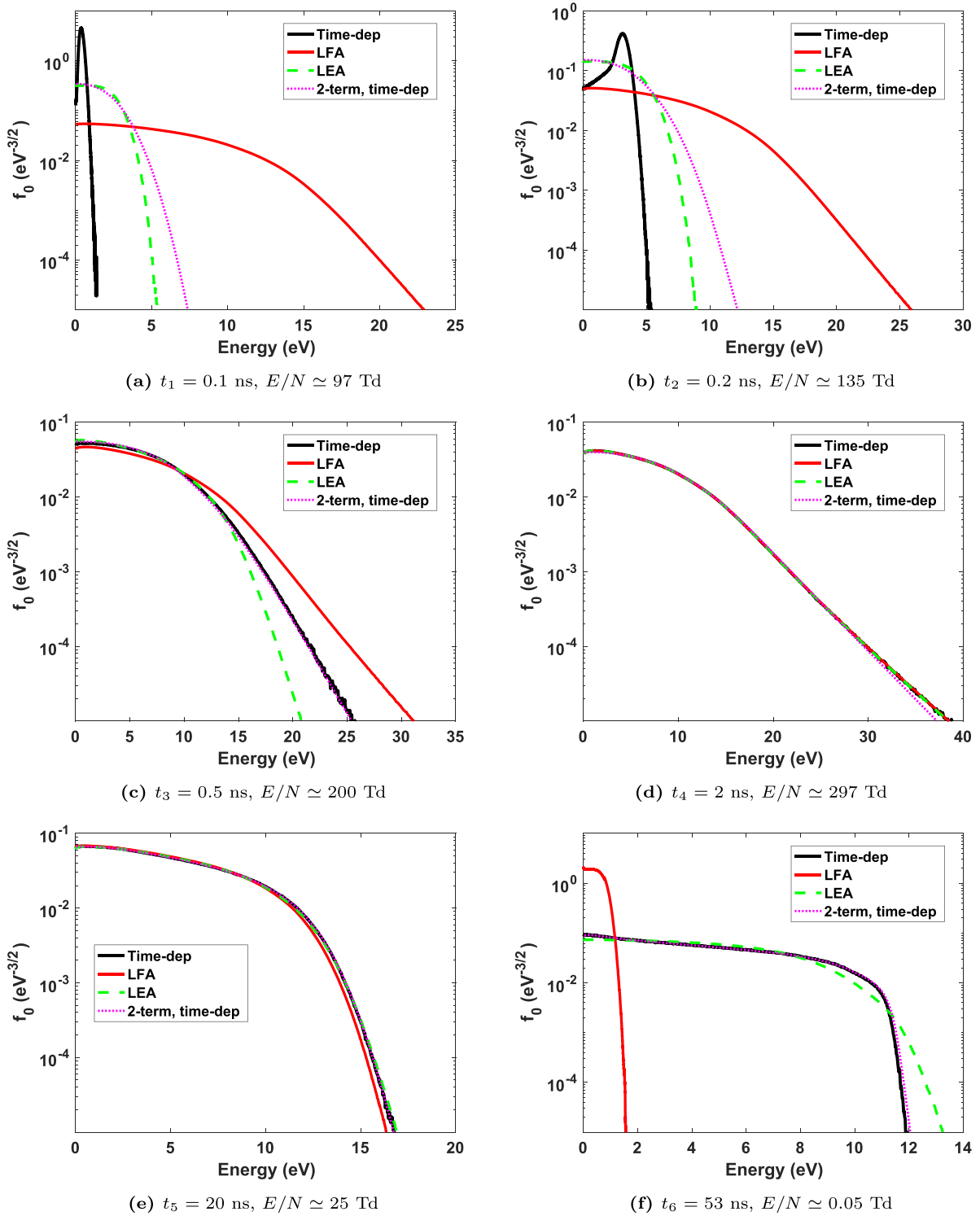


Figure 7. EEDFs in air, at 10 Torr, for different time instants  $t_1$ – $t_6$ .

pulses, the  $E/N$  pulse is repeated every  $\mu\text{s}$  during a total of  $8 \mu\text{s}$ . This repetition rate ensures various pulses within a short time period, but is shorter than typical experimental conditions. For all cases, the electron density ( $n_e$ ) is initialized to  $2.58 \times 10^{18} \text{ m}^{-3}$  and the initial gas temperature ( $T_g$ ) is 300 K. The chemical kinetic scheme involving  $\text{N}_2$ – $\text{O}_2$  species is taken from [50], including the updates on the oxygen kinetic scheme

from [51]. The reactions involving interactions between  $\text{N}_2$ – $\text{O}_2$  and Ar species are taken from [52].

The temporal evolution of the normalized electron density during the eight  $E/N$  pulses is shown in figure 9(a), for air at both 10 and 100 Torr, as well as for 10% air / 90% argon mixture at 100 Torr. For air at 10 Torr, the electron density is strongly underestimated by the LFA, while the LEA provides



**Figure 8.** EEDFs in argon, at 10 Torr, for different time instants  $t_1-t_6$ .

a good description. The unsuccess of the LFA under these conditions is primarily due to a stronger decay in electron density after the pulse, caused by an overestimation of dissociative recombination (main electron sink, see figure 3), which results in significantly different initial conditions for subsequent pulses. For air at 100 Torr, as collisionality increases, both the LFA and LEA provide good descriptions. However, for 10%

air / 90% argon at 100 Torr, the results of the LFA deviate once again from the accurate solution, while the LEA continues to provide a good description. This demonstrates that even at gas pressures near atmospheric levels, the LFA can be problematic when gas mixtures are mainly composed of atomic gases.

The temporal evolution of the normalized O-atom density for the same conditions is shown in figure 9(b). Inaccuracies

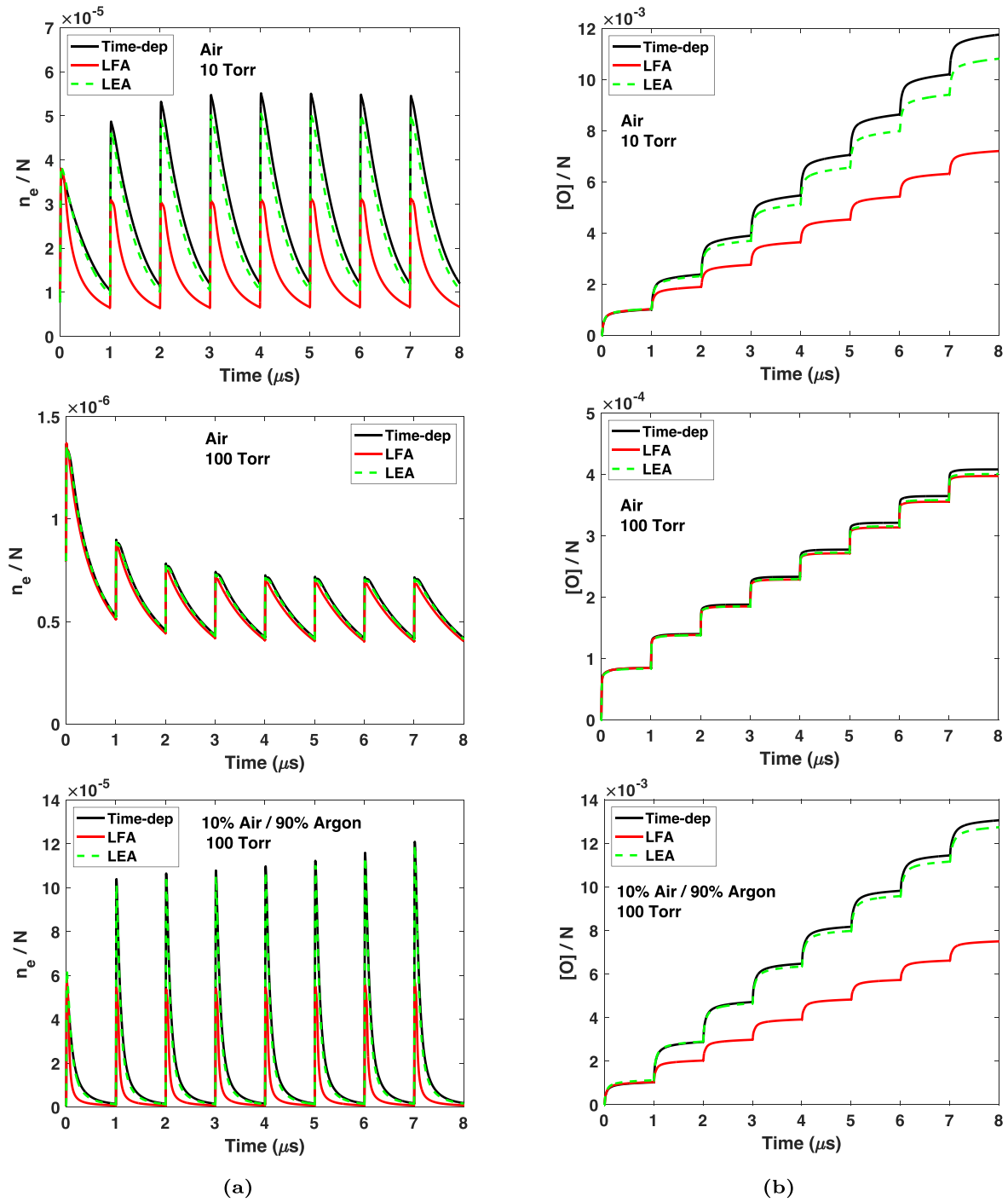


**Figure 9.** Temporal evolution of the normalized (a) electron density and (b) O-atom density, under three distinct conditions: air at 10 Torr, air at 100 Torr, and 10% air / 90% argon at 100 Torr. The solutions using the inputs from the LFA and LEA are compared against the accurate time-dependent solution.

in the electron density calculations subsequently lead to errors in the O-atom density that accumulate pulse after pulse. For air at 10 Torr and for 10% air / 90% argon mixture at 100 Torr, these errors are significant, whereas for air at 100 Torr, they remain minimal.

Figure 10 summarizes the errors of the LFA and LEA, relative to the accurate solution, on the production of various RONS, under the three different conditions. The errors

among different species are similar, which confirms that the temporal evolutions of O-atom densities exemplify well the discrepancies between the different approaches. Moreover, for (a) air at 10 Torr and (c) 10% air / 90% argon at 100 Torr, the LFA errors can reach  $\sim 40\%$ – $50\%$ , whereas the LEA errors are generally below 10%. This emphasizes the success of the LEA over the LFA in conditions of weak relaxation.

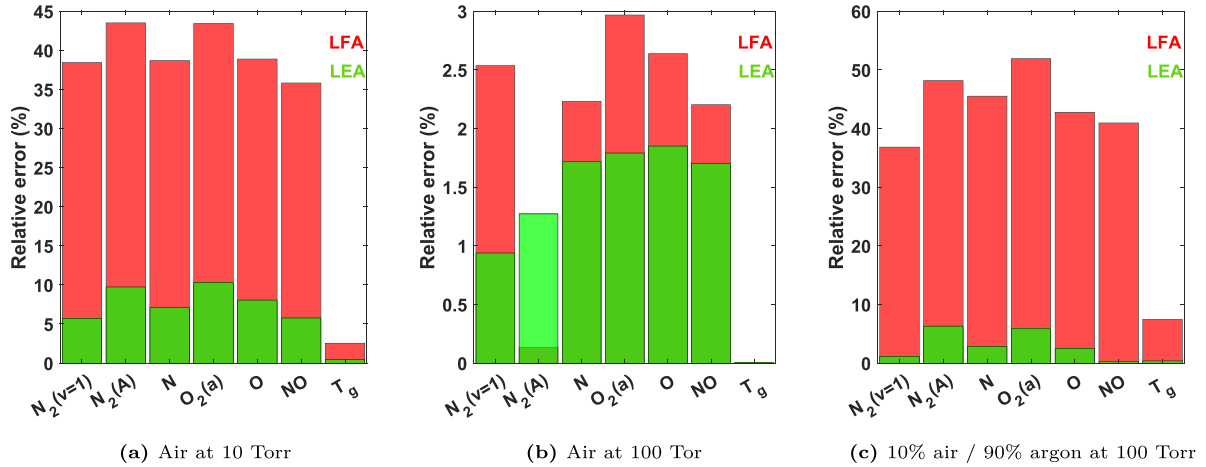


**Figure 10.** Summary of the errors of the LFA and LEA, relative to the accurate solution, of reactive oxygen and nitrogen species, after eight pulses.

#### 4. Final remarks

This investigation explored various techniques for modeling homogeneous electron kinetics in time-dependent  $E/N$  pulses, including: the rigorous time-dependent MC method, the LFA, the LEA, and the two-term time-dependent method. The steady-state results of the electron kinetics, supporting the LFA and LEA approaches, were obtained through accurate MC calculations to ensure that any deviations arose from temporal non-locality. This study focused on the electron relaxation within typical nanosecond pulses, considering different background gases (air, argon and mixtures of both) and two pressures (10 and 100 Torr).

A comparison with accurate time-dependent MC solutions clearly shows that, in general, the LEA provides more accurate results than the LFA. This improvement in accuracy can be attributed to the temporal effects incorporated through the equation for the mean electron energy in the LEA, which are absent in the LFA. Therefore, under weak relaxation conditions, and when a purely kinetic approach is not feasible, the LEA should be preferred over the LFA. This recommendation is in line with other investigations in the community [6, 7].

Since the LFA is commonly used, it is important to emphasize the potential impacts of this approximation on the results accuracy, specially at lower pressures or when atomic gases are abundantly present. During the initial nanosecond, the excessively fast relaxation predicted by the LFA leads to an overestimation of electron energy, which in turn results in an overvaluation of electron-impact ionization, dissociation and excitation. The repercussions of the LFA can be even more pronounced during the late-decay phase of the pulse. As  $E/N$  vanishes, the LFA predicts a strong decrease of electron energy, but energy relaxation might not be fast enough to adapt to the field reduction. This inaccuracy is critical because the electron density can remain elevated for a considerable

time after the pulse, influencing the heavy-species chemistry. For example, the LFA can strongly overestimate dissociative recombination, a significant path for electron loss. This, in turn, impacts the overall chemistry of heavy species. In repetitively-pulsed discharges, the accumulation of these systematic errors after each pulse can result in substantial deviations in model predictions, reaching up to 50% after eight pulses in the test cases considered in this work. However, we should stress that for gas mixtures dominated by molecular gases at pressures near atmospheric levels, both the LFA and LEA remain relatively accurate.

We should also note that fluid models employing the LEA can be numerically more expensive than the ones employing the LFA, since the treatment of the electron heating and collision terms often leads to numerical stiffness, requiring the usage of smaller time steps and/or sophisticated implicit solvers. Moreover, there might be cases where the required input cross sections for the LEA are not available, whereas electron swarm data (ionization frequencies, velocities and diffusion coefficients) can be extracted from pulsed or steady-state Townsend experiments, enabling the usage of the LFA but not the LEA [53].

We have demonstrated that a detailed comparison between the characteristic frequencies of momentum transfer and energy relaxation, combined with the rate of  $E/N$  variation, can delineate *a priori* the domains of validity for time-locality approximations, such as the LFA and LEA. The LFA is inaccurate in regions where the condition (2) is not verified, while the LEA is inaccurate (at least) in regions where the condition (5) is not verified. Temporal discrimination is fundamental in this examination, as mean electron energies and, consequently, mean relaxation frequencies, vary significantly over time. Concerning spatial variations, the analysis can be done similarly by comparing the mean free-path for energy and momentum relaxation with the characteristic lengths for spatial variation.

The comparison is extended to a two-term time-dependent solution with a quasi-stationary approximation for the first anisotropy  $f_1$ . Notably, at the lower pressure of 10 Torr, the two-term approach fails to capture the initial transient non-equilibrium. However, at later times, momentum transfer becomes faster than the field variation,  $f_1$  approximates stationarity, and the assumption holds. Similar conclusions have been reported, for example, by [17] and by Vialletto in chapter 2 of [54]. An analogous behavior is observed for the LEA method, which relies on steady-state mobilities parameterized as a function of mean electron energy.

To simplify the analysis, this study did not account for the influence of electron–electron and electron–ion collisions on the electron kinetics, although these processes can be incorporated into any of the formulations tested here. Under conditions of high ionization degrees ( $\sim 10^{-4} - 10^{-3}$ ), Coulomb collisions may significantly enhance energy relaxation efficiency. In such scenarios, the LFA and LEA are expected to provide descriptions that are equal to or better than those presented here. In particular, the enhancement of the electron energy diffusion due to electron–electron collisions should smooth the transient features in the EEDFs (see figure 7(e)), thereby improving the agreement between the LEA and the accurate time-dependent description. Work is in progress to investigate the effects of electron–electron and electron–ion interactions on the time-dependent electron kinetics.

We should mention that for nanosecond discharges with strong reduced electric fields, typically above 300 Td, the electron velocity distribution can become strongly anisotropic and nonlocal due to the continuous acceleration of high-energy electrons, leading to the phenomenon known as runaway electrons [55–57]. Approximations such as the LFA, the LEA or the two-term expansion are inadequate for describing these effects. To capture them accurately, a detailed kinetic description, such as the MC formulation within LoKI-MC used in this work, is necessary [55].

Finally, we wish to express a differing opinion from that reported in a recent note by [58], where the authors state that ‘the apparent reliability of calculations within the framework of the local-mean-energy approximation model for a number of parameters, in our opinion, only slows down progress in modeling of gas discharge plasma.’ From our perspective, the LEA remains a powerful method to describe the spatiotemporal electron kinetics in low-temperature plasmas and is valid across a wide range of conditions. The same can be argued for the LFA. In fact, many significant scientific and technological advancements in gas discharges over the past decades have relied on accurate predictions from these models [9, 28, 38–46, 48], enabling the simulation of conditions where a particle-in-cell + Monte-Carlo approach would be computationally unfeasible. Naturally, the LEA may not yield reliable results in regions where the mean free path for electron momentum transfer exceeds the characteristic length for spatial variations, such as in short glow discharges at low gas pressures, but that does not diminish its merit in a wide range of other conditions.

## Data availability statement

All data that support the findings of this study are included within the article (and any supplementary files).

## Acknowledgments

This work was supported by the Portuguese FCT–Fundação para a Ciência e a Tecnologia, under projects UIDB/50010/2020 (<https://doi.org/10.54499/UIDB/50010/2020>), UIDP/50010/2020 (<https://doi.org/10.54499/UIDP/50010/2020>), LA/P/0061/2020 (<https://doi.org/10.54499/LA/P/0061/2020>), PD/BD/150414/2019 (PD-F APPLAuSE) and PTDC/FIS-PLA/1616/2021 (PARADiSE, <https://doi.org/10.54499/PTDC/FISPLA/1616/2021>).

## ORCID iDs

Tiago C Dias  <https://orcid.org/0000-0002-2179-1345>  
Vasco Guerra  <https://orcid.org/0000-0002-6878-6850>

## References

- [1] Colonna G, Laricchiuta A and Pietanza L 2020 *Plasma Phys. Control. Fusion* **62** 014003
- [2] Tosi P, Montesano C, Quercetti S, Martini L M and Dilecce G 2020 *J. CO<sub>2</sub> Util.* **39** 101157
- [3] Šimek M and Bonaventura Z 2018 *J. Phys. D: Appl. Phys.* **51** 213001
- [4] Chng T L, Lepikhin N D, Orel I S, Popov N A, and Starikovskaia S M 2020 *Plasma Sources Sci. Technol.* **29** 035017
- [5] Brandenburg R, Bruggeman P and Starikovskaia S 2017 *Plasma Sources Sci. Technol.* **26** 020201
- [6] Dujko S, Markosyan A H, White R D and Ebert U 2013 *J. Phys. D: Appl. Phys.* **46** 475202
- [7] Grubert G K, Becker M M and Loffhagen D 2009 *Phys. Rev. E* **80** 036405
- [8] Becker M and Loffhagen D 2013 *Adv. Pure Appl. Math.* **3** 343–52
- [9] Salabas A, Gousset G and Alves L L 2002 *Plasma Sources Sci. Technol.* **11** 448
- [10] Boeuf J P and Pitchford L C 1995 *Phys. Rev. E* **51** 1376–90
- [11] Hagelaar G J M and Pitchford L C 2005 *Plasma Sources Sci. Technol.* **14** 722–33
- [12] Markosyan A H, Teunissen J, Dujko S and Ebert U 2015 *Plasma Sources Sci. Technol.* **24** 065002
- [13] Viegas P, Slikboer E, Bonaventura Z, Guaitella O, Sobota A and Bourdon A 2022 *Plasma Sources Sci. Technol.* **31** 053001
- [14] Dias T C, Tejero-del-Caz A, Alves L L and Guerra V 2023 *Comput. Phys. Commun.* **282** 108554
- [15] Dias T C, Pintassilgo C D and Guerra V 2023 *Plasma Sources Sci. Technol.* **32** 095003
- [16] Boyle G J, Casey M J E, Cocks D G, White R D and Carman R J 2019 *Plasma Sources Sci. Technol.* **28** 035009
- [17] Loffhagen D and Winkler R 1996 *Plasma Sources Sci. Technol.* **5** 710
- [18] Trunec D, Španelglq P and Smith D 2003 *Chem. Phys. Lett.* **372** 728–32
- [19] Loffhagen D and Winkler R 1996 *J. Phys. D: Appl. Phys.* **29** 618
- [20] Winkler R, Loffhagen D and Sigenege F 2002 *Appl. Surf. Sci.* **192** 50–71

- [21] Trunec D, Bonaventura Z and Nečas D 2006 *J. Phys. D: Appl. Phys.* **39** 2544
- [22] Li Y M 1990 *Nonequilibrium Effects in Electron Transport at High E/n* (Springer US) pp 99–120
- [23] del Caz A T, Guerra V, Pinhão N, Pintassilgo C D and Alves L L 2021 *Plasma Sources Sci. Technol.* **30** 065008
- [24] Dhali S K 2022 *Plasma Sources Sci. Technol.* **31** 025014
- [25] Hoder T, Loffhagen D, Becker J V M M and Brandenburg R 2016 *Plasma Sources Sci. Technol.* **25** 025017
- [26] Bieniek M S, Walsh J L and Hasan M I 2021 *Phys. Plasmas* **28** 063501
- [27] White R, Robson R and Ness K 1999 *IEEE Trans Plasma Sci.* **27** 1249–53
- [28] Pokrovskiy G V, Popov N A and Starikovskaia S M 2022 *Plasma Sources Sci. Technol.* **31** 035010
- [29] Zhu Y, Lepikhin N D, Orel I S, Salmon A, Klochko A V and Starikovskaia S M 2018 *Plasma Sources Sci. Technol.* **27** 075020
- [30] Vasilyak L M, Kostyuchenko S V, Kudryavtsev N N and Filyugin I V 1994 *Phys.-Usp.* **37** 247
- [31] Takashima K, Adamovich I V, Xiong Z, Kushner M J, Starikovskaia S, Czarnetzki U and Luggenhölscher D 2011 *Phys. Plasmas* **18** 083505
- [32] Zhu Y, Starikovskaia S M, Babaeva N Y and Kushner M J 2020 *Plasma Sources Sci. Technol.* **29** 125006
- [33] N.d. IST-Lisbon database (available at: [www.lxcat.net](http://www.lxcat.net))
- [34] Yanguas-Gil A, Cotrino J and Alves L L 2005 *J. Phys. D: Appl. Phys.* **38** 1588
- [35] Alves L L, Coche P, Ridenti M and Guerra V 2016 *Eur. Phys. J. D* **70** 124
- [36] Coche P, Guerra V and Alves L L 2016 *J. Phys. D: Appl. Phys.* **49** 235207
- [37] Budde M, Dias T C, Vialetto L, Pinhão N, Guerra V and Silva T 2023 *J. Phys. D: Appl. Phys.* **56** 255201
- [38] Ferreira N G C, Santos D F N, Almeida P G C, Naidis G V and Benilov M S 2019 *J. Phys. D: Appl. Phys.* **52** 355206
- [39] Bourdon A, Pasko V P, Liu N Y, Célestin S, Ségur P and Marode E 2007 *Plasma Sources Sci. Technol.* **16** 656
- [40] Boeuf J-P 1987 *Phys. Rev. A* **36** 2782–92
- [41] Norberg S A, Johnsen E and Kushner M J 2015 *Plasma Sources Sci. Technol.* **24** 035026
- [42] Park S and Economou D J 1990 *J. Appl. Phys.* **68** 3904–15
- [43] Nienhuis G J, Goedheer W J, Hamers E A G, van Sark W G J H M and Bezemer J 1997 *J. Appl. Phys.* **82** 2060–71
- [44] Lymberopoulos D P and Economou D J 1995 *J. Phys. D: Appl. Phys.* **28** 727
- [45] Nitschke T E and Graves D B 1994 *J. Appl. Phys.* **76** 5646–60
- [46] Gogolides E and Sawin H H 1992 *J. Appl. Phys.* **72** 3971–87
- [47] Tejero-del-Caz A, Guerra V, Gonçalves D, Lino da Silva M, Marques L, Pinhão N, Pintassilgo C D and Alves L L 2019 *Plasma Sources Sci. Technol.* **28** 043001
- [48] Makabe T, Nakano N and Yamaguchi Y 1992 *Phys. Rev. A* **45** 2520–31
- [49] Dujko S, Raspopović Z M and Petrović Z L 2005 *J. Phys. D: Appl. Phys.* **38** 2952
- [50] Guerra V, Tejero-del Caz A, Pintassilgo C D and Alves L L 2019 *Plasma Sources Sci. Technol.* **28** 073001
- [51] Dias T C, Fromentin C, Alves L L, del Caz A T, Silva T and Guerra V 2023 *Plasma Sources Sci. Technol.* **32** 084003
- [52] Gaens W V and Bogaerts A 2013 *J. Phys. D: Appl. Phys.* **46** 275201
- [53] Petrović Z L, Dujko S, Marić D, Malović G, Nikitović Ž, Šašić O, Jovanović J, Stojanović V and Radmilović-Radjenović M 2009 *J. Phys. D: Appl. Phys.* **42** 194002
- [54] Vialetto L 2021 *PhD Dissertation Applied Physics and Science Education*, Eindhoven University of Technology
- [55] Moss G D, Pasko V P, Liu N and Veronis G 2006 *J. Geophys. Res. Space Phys.* **111** A02307
- [56] Tarasenko V 2020 *Plasma Sources Sci. Technol.* **29** 034001
- [57] Contreras-Vidal L, d. Silva C L and Sonnenfeld R G 2022 *J. Phys. D: Appl. Phys.* **56** 055201
- [58] Zhou C, Rafatov I, Wang Y, Kudryavtsev A, Yuan C, Yao J and Zhou Z 2024 *Plasma Sources Sci. Technol.* **33** 077001